2011 American Control Conference
on O'Farrell Street, San Francisco, CA, USA
June 29 - July 01, 2011

Modeling and Feedforward Control of a Large-Range, Piezo Nano-Stepper

Scott Wilcox and Santosh Devasia
Department of Mechanical Engineering, University of Washington

Abstract— **This article aims to improve the positioning performance of piezo-based nano-steppers, which have both large range and high-precision. The main contribution of this article is to show that model-based feedforward input can improve the performance of piezo-based nano-steppers by enabling operation at higher frequencies.**

I. INTRODUCTION

The article aims to improve the performance of piezo-based nano-steppers. Starting with the initial design in [1], nano-steppers, such as those using stick-slip actuation, enable nanoscale precision over relatively large range — by making multiple nanoscale steps, e.g., [2]-[8]. A challenge with nano-steppers is to minimize the effect of the stepping process on the positioning, e.g., to reduce the variation in positioning velocity during each stepping motion. Such velocity variations are lower at higher operating frequencies, provided the piezo can be positioned accurately. However, unwanted vibrations, can lead to substantial errors in the desired piezo positioning at higher frequencies, which in turn can lead to increased positioning error in the nano-stepper. The main contribution of this article is to show that model-based feedforward input can improve the performance of piezo-based nano-steppers by accounting the dynamics-caused vibrations and thereby enabling operation at higher frequencies. Towards this, a model of the nano-stepper is developed and inverted to find feedforward inputs that correct for the vibrational effects.

It is challenging to achieve large-range and high-bandwidth simultaneously with piezo-type actuators. Note that typical smart-material actuators can achieve precision positioning over relatively-large, hundreds-of-microns range. The difficulty is that the mechanical, vibrational-resonance frequencies of the positioner (and therefore, those of the system that uses the positioner) tend to be lower for large-range smart-material actuators. System zeros tend to be interlaced between these vibrational-resonance frequencies [9] — and they tend to be fundamental limits to increasing bandwidth. Note that advanced control techniques can help to reduce the vibrations and thereby improve the bandwidth (operating speed) of nanopositioners, e.g., see a recent review in [10]. In particular, starting with the early work in [11], modern control techniques, e.g. [12]-[15], have enabled an increase in the operating speed of general nanopositioners.

Nevertheless, zeros in the system imply that the system does not have sufficient response, just after the first vibrational-resonance frequency ω_1. Therefore, input saturation can limit the ability to drive the piezo-actuator (with sufficient output response) beyond ω_1 for general trajectories. (*Although specific trajectories, such as sinusoids at the second vibrational-resonance frequency, could still be tracked.*) The challenge of achieving both large-range and high-bandwidth has received substantial interest from the research community, e.g., with novel design approaches such as flexural-lever arms that amplify a piezo-actuator's displacement while minimizing the accompanying reduction in stiffness [16]-[18].

Nano-steppers can increase range without loss of bandwidth because they can achieve large-range positioning by making multiple steps with its actuators. The amplitude of each stepping motion of the actuator can be small in comparison to the overall range. Therefore, relatively smaller actuators can be used in nano-steppers in comparison to a single large actuator. Smaller actuators tend to have higher resonant-vibrational frequencies, which tends to effectively increase the achievable bandwidth. Moreover, when a relatively-stiff positioner is needed (to avoid undesirable vibration effects), it is advantageous to use nano-steppers rather than increasing the range by using larger actuators. An additional advantage of nano-steppers is that they can be designed to hold a position without the use of active inputs, which is important in applications where the changes in position are only required once in a while and the available input is limited. Finally, nano-steppers can be used as one of the positioners in standard dual-stage approaches to nanopositioning (e.g., [19], [20]) that are used to increase the precision and range.

The challenge with nano-steppers is that, during each step, movement-induced vibrations can lead to positioning errors in the actuators used in the nano-steppers. These positioning errors, in turn, lead to loss of positioning ability with the nano-stepper. This article develops a model of a nano-stepper and inverts the dynamics to find feedforward inputs [21] to correct for the vibrational effects, and thereby, potentially improve the positioning performance.

II. SYSTEM DESCRIPTION

The nano-stepper (see Fig. 1) body is constructed of two acrylic L-shaped panels, each with three (Lead-Zirconate-Titanate (PZT)) piezoelectric, bimorph actuators acting as legs for the system. The actuators move in a bending fashion similar to canitilever beams. Control signals, generated from a PC by using a Digital-to-Analog (D/A) card, are applied to the piezo actuators through a voltage amplifier. The nano-stepper runs along a track with sides that restrict it to move,

978-1-4577-0079-8/11/$26.00 ©2011 AACC

forward or backward, along a single axis.

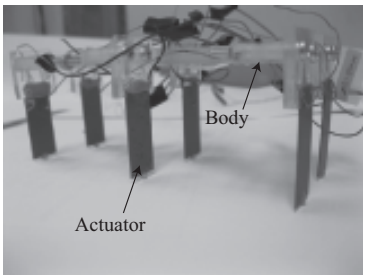

Fig. 1. Photo of six-legged nano-stepper.

Motion Generation Motion is generated using the friction force F between the piezo-actuator tip and the ground as the piezo-actuator is deflected back and forth as illustrated in Fig. 2(top). For example, during the backward motion (negative velocity) of the piezo-actuator tip, over the time interval $(0, T^*)$, the friction force F is positive as shown in Fig. 2. Similarly, during the forward motion (positive velocity) of the piezo-actuator tip, over the time interval (T^*, T) the friction force F, is negative. The only significant external force acting in the horizontal direction on the nano-stepper is this friction force F, and therefore, the motion of the center of mass X_{cm} of the nano-stepper is given by

$$M_t \frac{d^2}{dt^2} X_{cm}(t) = F(t) \tag{1}$$

where M_t is the total mass of the system.

Problem The motion of the center of mass X_{cm} depends on the friction force $F(t)$ (from Eq. 1), which in turn, depends on the velocity of the piezo-actuator tip. As the actuation frequency (of the back-and-forth motion of the piezo-actuator) increases, excitation of the vibrational dynamics of the piezo-actuator leads to unwanted changes in the tip-velocity direction, and therefore, leads to loss of control over the motion of the nano-stepper.

III. THEORETICAL MODEL

A model of the piezo-actuator dynamics, was developed as the bending $w(x,t)$ of a cantilever beam attached to the main body that was modeled as a lumped mass M_b whose position is $u(t)$. Then, the net position $\hat{y}(x,t)$ of a point x on the piezo-actuator is given by the sum of the main body motion $u(t)$ and the deflection $w(x,t)$ of the piezo-actuator, i.e.,

$$\hat{y}(x,t) = w(x,t) + u(t) \tag{2}$$

where the bending dynamics is given by the Euler-Bernoulli beam approach as, e.g., [22],

$$\rho A \frac{\partial^2 \hat{y}}{\partial t^2} + EI \frac{\partial^4 \hat{y}}{\partial x^4} = f(x,t) \tag{3}$$

where ρ is the density, A is the cross sectional area, E is the elastic modulus, and I is the moment of inertia of the piezo- actuator.

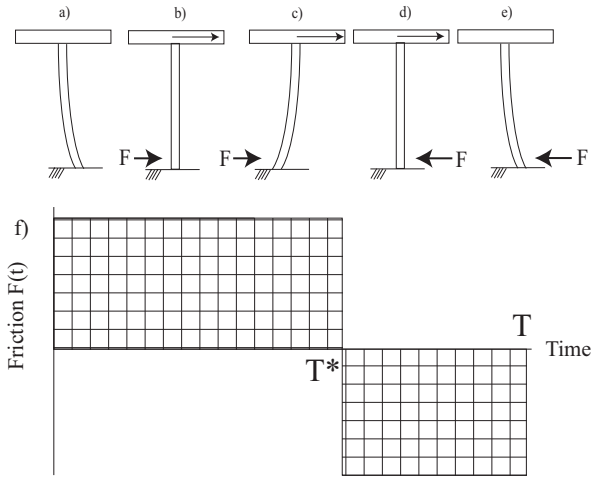

Fig. 2. Motion of the actuator and friction direction: a) actuator in the forward position; b)-c) as the actuator moves backward, a positive friction force, F, is generated until time T^*; d)-e) the actuator returns to the forward position generating a negative friction force, F; and f) the friction force F during each period T — the pattern of actuator motion and friction direction repeats with periodicity T.

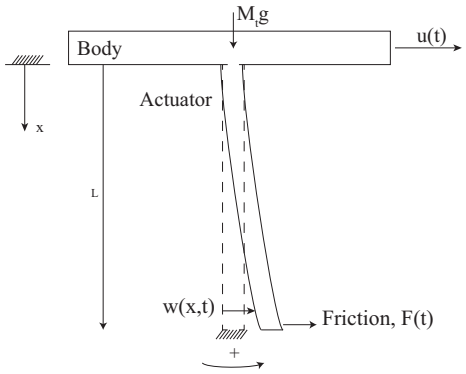

Fig. 3. Free body diagram: the only external force in the lateral direction is the friction force F

The piezo-actuator deflection w is split into its modal components, with separated spatial X and temporal T parts, as

$$w(x,t) = \sum_{1}^{\infty} X_n(x) T_n(t) \tag{4}$$

and the beam dynamics (Eq. 3) is rewritten as

$$\sum_{1}^{\infty} \left[\rho A \ddot{T}_n(t) X_n(x) \; + EI T_n(t) X_n^{(4)}(x) \right] = f(x,t) - \rho A \ddot{u}(t) \tag{5}$$

The homogeneous form of equation (5), obtained by setting the right hand side to zero, can be solved using separation of variables and the boundary conditions for a standard cantilever beam:

$$w(0,t) = 0; \;\; w_x(0,t) = 0; \;\; w_{xx}(L,t) = 0; \;\; w_{xxx}(L,t) = 0$$

and L is the length of the piezo-actuator. This yields separate equations for the spatial X_n and temporal T_n portions of the

n^{th} mode

$$\frac{EI}{\rho A}\frac{X_n^{(4)}(x)}{X_n(x)} = \omega_n^2; \qquad \frac{\ddot{T}_n(t)}{T_n(t)} = -\omega_n^2, \tag{6}$$

with the spatial solution X_n given by [22],

$$X_n(x) = sin(\beta_n x) - sinh(\beta_n x) + \sigma_n(cos(\beta_n x) - cosh(\beta_n x))$$

where

$$\beta_n^4 = \frac{\omega_n^2 \rho A}{EI}; \qquad \sigma_n = \frac{sin(\beta_n L) + sinh(\beta_n L)}{cos(\beta_n L) + cosh(\beta_n L)}, \tag{7}$$

and for the first ($n = 1$) vibrational mode [22]

$$\beta_1 L = 1.875 \quad \text{and} \quad \sigma_1 = 0.7341.$$

Dynamics of First Vibrational Mode Using the orthogonality of the mode shapes, the first mode dynamics $X_1(x)$, is extracted by multiplying Eq. (5) by the first mode shape and integrating with respect to the beam length.

$$\sum_1^\infty \left[\int_0^L X_1 X_n \ddot{T}_n dx + \frac{EI}{\rho A} \int_0^L X_1 \beta_n^4 X_n T_n dx \right] = \frac{1}{\rho A} \int_0^L X_1 r(x,t) dx \tag{8}$$

to yield

$$\ddot{T}_1 + \omega_1^2 T_1 = \frac{1}{\rho A} \frac{\int_0^L X_1 r(x,t) dx}{\int_0^L X_1 X_1 dx}. \tag{9}$$

where the forcing term r in Eq. (8) is given by

$$r(x,t) = M(t)\frac{\partial \delta(x-L)}{\partial x} + F(t)\delta(x-L) + \rho A \ddot{u}(t) \tag{10}$$

where $M(t)$ is the applied moment due the voltage V acting on the piezo-actuator, $F(t)$ is the friction force acting on the piezo-actuator tip and $\ddot{u}(t)$ is the acceleration of the main body (see Fig. 3). Integrating, Eq. (9), can be rewritten as

$$\begin{aligned} \ddot{T}_1 + \omega_1^2 T_1 &= \frac{\overline{X_1}}{\overline{X_1^2}}\ddot{u}(t) + \frac{X_1(L)}{\rho A \overline{X_1^2}} F(t) \\ &\quad + \frac{\partial X(x)/\partial x|_{x=L}}{\rho A \overline{X_1^2}} M(t) \qquad (11) \\ &= K_1 \ddot{u}(t) + K_2 F(t) + K_3^* M(t) \qquad (12) \end{aligned}$$

where

$$\overline{X_1} = \int_0^L X_1(x) dx \quad \text{and} \quad \overline{X_1^2} = \int_0^L X_1(x) X_1(x) dx. \tag{13}$$

A relation between the moment M generated by an applied voltage V can be obtained as

$$\begin{aligned} M(t) &= \frac{2EI}{L^2} Y(t) \quad \text{from [23]} \\ &= \frac{2EI}{L^2}\left(3 d_{31} \frac{L^2}{T^2} V(t)\right) \quad \text{from [24]} \\ &= \frac{6 d_{31} EI}{T^2} V(t) \qquad (14) \end{aligned}$$

where $Y(t)$ is the piezo-tip deflection for an applied voltage $V(t)$, T is the thickness of the piezo-actuator and d_{31} is a piezoelectric coefficient. Substituting for the moment $M(t)$ (in Eq. 14) into the dynamics of the first mode (in Eq. 12) and adding a damping term, the first-mode dynamics can be rewritten as

$$\ddot{T}_1 + 2\zeta_1 \omega_1 \dot{T}_1(t) + \omega_1^2 T_1 = K_1 \ddot{u}(t) + K_2 F(t) + K_3 V(t) \tag{15}$$

where

$$K_3 = \frac{6 d_{31} EI}{T^2} K_3^* \tag{16}$$

and ζ_1 is the damping ratio. With the one-vibrational-mode model, the piezo-tip motion $Y(t)$ can be described as

$$Y(t) = X_1(L) T_1(t) \tag{17}$$

Substituting the above into Eq. 15, gives

$$\ddot{Y}(t) + 2\zeta_1 \omega_1 \dot{Y}(t) + \omega_1^2 Y(t) = \frac{K_1}{X_1(L)}\ddot{u}(t) + \frac{K_2}{X_1(L)} F(t) + \frac{K_3}{X_1(L)} V(t). \tag{18}$$

Since most of the mass is located in the body, the position of the center of mass X_{cm} can be approximated as the position of the body, $u(t)$. This substitiution alters Eq. (1) to

$$M_t \ddot{u}(t) = F(t), \tag{19}$$

where the friction force, $F(t)$, is taken to be coulomb friction given by

$$F(t) = -\mu_k M_t g \; Sign(\dot{Y}(t)). \tag{20}$$

Dynamics of Piezo The focus of this article is on the control of the piezo, and its potential effects on the nano-stepper motion. Towards this, the friction nonlinearities were removed by raising the system above ground (i.e., $F(t) = 0$), and clamping the top body (in Fig. 1), to isolate the piezo dynamics, which reduces to (from Eq. 18)

$$\ddot{Y}(t) + 2\zeta_1 \omega_1 \dot{Y}(t) + \omega_1^2 Y(t) = \frac{K_3}{X_1(L)} V(t). \tag{21}$$

Using Laplace transform, the transfer function is

$$\begin{aligned} G(s) = \frac{Y(s)}{V(s)} &= \frac{K_3/X_1(L)}{s^2 + 2\zeta_1\omega_1 s + \omega_1^2} \\ &= \frac{K_{DC}\ \omega_1^2}{s^2 + 2\zeta_1\omega_1 s + \omega_1^2}. \end{aligned} \tag{22}$$

IV. EXPERIMENTAL PIEZO MODEL

The parameters of the piezo model (in Eq. 22) were obtained experimentally. Towards this, the nano-stepper was suspended above the track and a Kalman SMU-9000-15N inductive sensor was used to measure the piezo-tip deflection, for different sinusoidal inputs, generated using a Stanford Research Systems Digital Signal Analyzer. Experimental bode plots of the system, for different amplitudes A_V of the input voltage V, are shown in Fig. 4.

Although, piezos have infinite modes of vibration, the Bode plots in Fig. 4 suggest that a second-order model would be sufficient. The fitted model parameters are shown in Table I. There is a small change in the experimental natural frequency

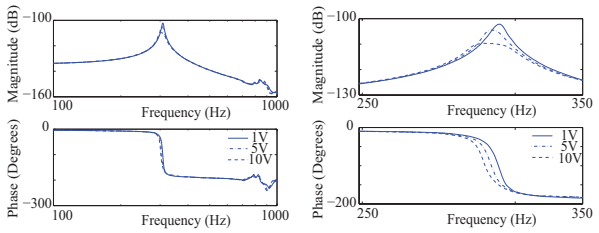

Fig. 4. Experimental Bode plots for different input amplitudes A_V.

ω_1 with increasing input-voltage amplitude, however, there is a larger influence of the input-voltage amplitude on the damping ratio, which could be attributed to hysteretic damping effects in piezo actuators. The fitted models compare well against the experimental results, as seen in Fig. 5 for the $1V$ input amplitude case — the fitted model is accurate until $\approx$700 Hz.

TABLE I

MODEL PARAMETERS FOR DIFFERENT INPUT V AMPLITUDES (A_V)

Amplitude A_V	ω_1 (Hz)	ζ	$K_{DC}(dB)$
1	307	0.0119	-134.95
5	305	0.0134	-135.04
10	303	0.0179	-135.16

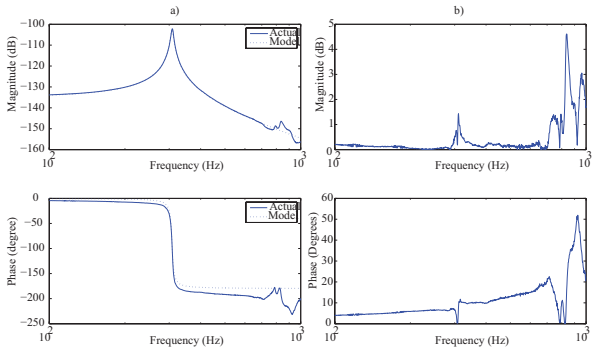

Fig. 5. a) Comparison of Bode plots from Experiment and (fitted) Model for input amplitude of $A_v = 1V$ b) Error between Bode plots of (fitted) model and experiment

V. TRAJECTORY DESIGN

The external force applied on the nano-stepper, i.e., the friction force with the ground, depends on the direction of the tip velocity. Therefore, it is important to precisely control to piezo-tip velocity to control the overall forces, and thereby, to control the positioning precision of the nano-stepper.

Choice of Trajectory Asymmetry While, a variety a trajectories could be chosen, a polynomial approach is used in the following. In particular, the velocity trajectory was chosen to be a composite of two polynomials: (i) a negative-time polynomial $V_n(t)$ for time $t \in [-T_n, 0]$; and (ii) a positive-time polynomial $V_p(t)$ over time $t \in [0, T_p]$ as shown in as shown in Fig. (6). The time intervals T_n and T_p are related to the frequency of the input period (T in Fig. 2) by

$$T_n + T_p = T \tag{23}$$

$$T_n = \alpha T \tag{24}$$

where the ratio α determines the amount of asymmetry in the piezo displacement Y (in Fig. 6).

Design of Trajectory The following four continuity constraints are placed on the velocity polynomials (and its derivatives) to avoid rapid changes in the acceleration, which can require large spikes in the inputs that can, in turn, excite unwanted higher-order modes of vibration.

$$\begin{array}{rcl} V_n(0) & = & V_p(0) \\ V_n(-T_n) & = & V_p(T_p) \\ \frac{d}{dt}V_n(0) & = & \frac{d}{dt}V_p(0) \\ \frac{d}{dt}V_n(-T_n) & = & \frac{d}{dt}V_p(T_p) \end{array} \tag{25}$$

The constraints are satisfied by the following 4^{th} order polynomial

$$V_p = -(t - T_p)^2 t^2 S_p \tag{26}$$

$$V_n = (t - T_n)^2 t^2 S_n \tag{27}$$

where the scaling factors S_p, S_n are chosen to achieve the desired maximum displacement Y_{max}, i.e.,

$$\begin{array}{rcl} Y_{max} & = & -\int_0^{T_p} V_p(t)dt \\ Y_{max} & = & \int_{-T_n}^{0} V_n(t)dt. \end{array} \tag{28}$$

The above constraints on the maximum displacement Y_{max} results in

$$S_n = \frac{30 Y_{max}}{T_n^5}; \qquad S_p = \frac{S_n T_n^5}{T_p^5}. \tag{29}$$

To illustrate, the velocity trajectory for the $\alpha = 25\%$ asymmetry (in Eq. 24) gives the following two equations:

$$V_n = (3.24e7)(t^4 - 2T_n t^3 + T_n^2 t^2) \tag{30}$$

$$V_p = -(1.33e5)(t^4 - 2T_p t^3 + T_p^2 t^2) \tag{31}$$

The corresponding position $Y(t)$, velocity $\dot{Y}(t)$ and acceleration $\ddot{Y}(t)$ trajectories are shown in Fig. 6.

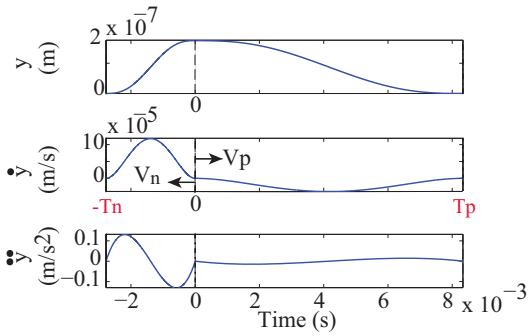

Fig. 6. Piezo-tip position Y, velocity $\dot{Y}$, and acceleration $\ddot{Y}$ profiles

VI. TRAJECTORY TRACKING

The model in Eq. (21) was inverted to find the inverse input V_{inv} as

$$V_{inv}(t) \;=\; \frac{X_1(L)}{K_3}\left[\ddot{Y}_d(t) + 2\zeta_1\omega_1\dot{Y}_d(t) + \omega_1^2 Y_d(t)\right]. \quad (32)$$

This inverse input V_{inv} was applied to the experimental piezo system for several different values of asymmetry α, i.e., $\alpha \in (25\%, 30\%, 40\%, 45\%)$. The frequency of the periodic desired trajectory Y_d was chosen as 90 Hz so that the higher harmonics would miss the resonance frequency, where positioning errors can be expected due to hysteresis dependent errors (as in Fig. 4). The tracking results for position are shown in Fig. 7 and in Fig. 8 for velocities — the tracking errors are shown in Table II, where

$$\begin{aligned} e_y &= \max_{t\in[0,T]} |Y(t) - y_d(t)| \quad (33)\\ e_{\dot{y}} &= \max_{t\in[0,T]} |\dot{Y}(t) - \dot{y}_d(t)| \\ \%e_y &= \frac{e_y}{Y_{max}} \\ \%e_{\dot{y}} &= \frac{e_{\dot{y}}}{\max_{t\in[0,T]} |\dot{y}_d|}. \end{aligned}$$

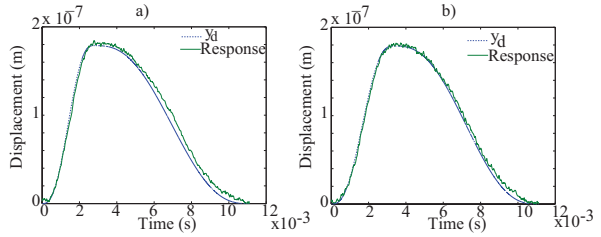

Fig. 7. Comparison of desired position Y_d and experimental position Y for: (a) $\alpha = 25\%$ asymmetry; and b) $\alpha = 30\%$ asymmetry.

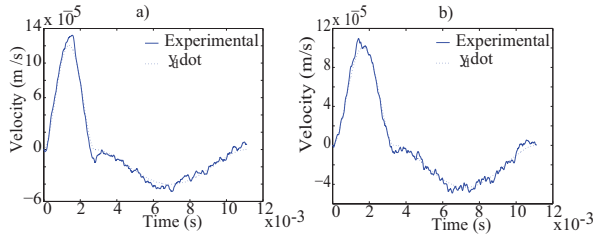

Fig. 8. Comparison of desired velocity $\dot{Y}_d$ and experimental position $\dot{Y}$ for: (a) $\alpha = 25\%$ asymmetry; and b) $\alpha = 30\%$ asymmetry.

TABLE II

TRACKING ERRORS (EQ. 33) FOR DIFFERENT ASYMMETRY α

α	e_y	$\%e_y$	$e_{\dot{y}}$	$\%e_{\dot{y}}$
25	6.82E-09	2.55	1.65E-05	11.73
30	4.67E-09	2.61	1.38E-05	13.77
35	2.32E-09	1.29	8.97E-06	10.4
40	5.86E-09	3.28	2.09E-05	27.7
45	3.68E-09	2.06	8.76E-06	13.07

VII. STEADY-STATE VELOCITY ESTIMATION

Using the velocity of the piezo-tip, the steady state velocity (V_{ss}) of the nano-stepper can be obtained by matching the time interval over which the friction force F is positive (i.e., total tip velocity $V_{net}(t)$, where

$$V_{net}(t) = \dot{Y}(t) + \dot{u}(t)$$

is negative) to be the same as the time interval over which the friction force F is negative (i.e., total tip velocity $V_{net}(t)$ is positive). This can be found by effectively shifting the velocity of the tip in Fig. 9(a) by the steady state value

$$V_{ss} = -V_p(\beta) \quad (34)$$

and equating the time interval over which the net velocity is positive and where the net velocity is negative, i.e., from Fig. 9(a),

$$(T - T_3) + (T_2 - 0) \;=\; (T_3 - T_2) \quad (35)$$

which leads to

$$\alpha T + 2\beta = T_3 - T_2 \quad (36)$$

with β given by

$$\beta = T\left[\frac{1}{4} - \frac{\alpha}{2}\right]. \quad (37)$$

The steady state velocity V_{ss} can then be found from Eq. 34 and is plotted for different asymmetry α in Fig. 10.

Nano-stepper Velocity V_{ss} Control Note that the steady state velocity tends to zero as the position trajectory Y_d becomes more symmetric. Similarly, the experimentally expected steady-state velocity can be estimated by using the experimental velocity data; the experimental estimation of the steady-state velocity is compared to the model-based steady-state velocity in Fig. 10, and the difference is tabulated in Table. III. As seen from these results, the velocity of the nano-stepper could be effectively adjusted by using different asymmetry in the piezo-tip trajectory, which also provides an approach for feedback control of the nano-stepper.

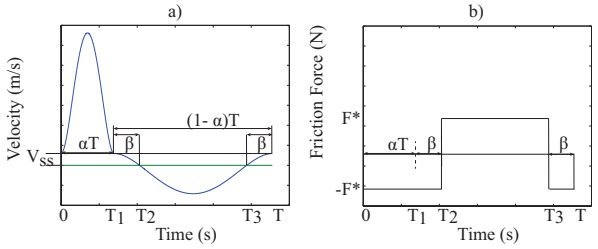

Fig. 9. a) Steady-state velocity V_{ss} estimation; b) Expected friction force with magnitude $F^* = \mu_k g M_t$

Need for high-frequency operation While the net impulse (of the friction force) over each time period T is zero at steady-state as in Fig. 9(b), the impulse is non-zero over any sub-interval of length less than T. The maximum variation

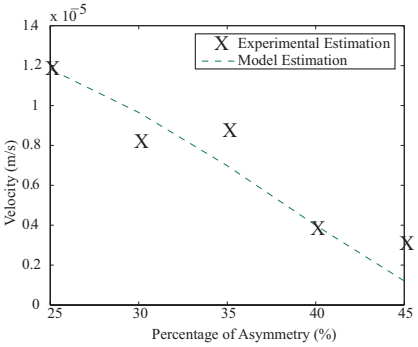

Fig. 10. Experimental and model-based estimates for steady-state velocity of nano-stepper V_{ss}

TABLE III

STEADY-STATE VELOCITY V_{ss} COMPARISON

Asymmetry α	Model Estimate	Experimental Estimate	Difference	Percent Difference
25	11.822e-06	12.014e-06	.192e-06	1.62
30	9.651e-06	8.042e-06	1.609e-06	16.67
35	6.976e-06	8.617e-06	1.637e-06	23.46
40	3.996e-06	3.694e-06	0.302e-06	7.54
45	1.206e-06	2.940e-06	1.734e-06	143.72

η of the nanostepper velocity $u(t)$ around the steady-state velocity V_{ss} is given by

$$\begin{aligned}\eta = \Delta\dot{u} &= u(T_3) - u(T_2) \\ &= \int_{T_2}^{T_3} \ddot{u}(t)dt \\ &= \int_{T_2}^{T_3} \frac{F(t)}{M_t}dt \\ &= \mu_k g(T_3 - T_2) \ = \mu_k g T/2\end{aligned} \tag{38}$$

This shows a linear relationship between the amount of variation η in the nano-stepper velocity and the period T of the piezo motion trajectory. Therefore, a higher frequency of piezo motion is desirable to reduce the amount of variation seen in the steady-state velocity of the body, provided precision tracking of the tip-position (rather the tip velocity) is achieved using controls. Our ongoing efforts are aimed at experimental verification of such control schemes for high-precision control of the nano-stepper over relatively-large range.

VIII. CONCLUSIONS

This article develops an inversion-based feedforward approach to improve the positioning performance of piezo-based nano-steppers, which have both large range and high-precision. The article showed that model-based feedforward input can be used to achieve velocity control of piezo-based nano-steppers by appropriately designing the asymmetry in the positioning trajectory.

IX. ACKNOWLEDGMENTS

The authors gratefully acknowledge the following grants from the National Science Foundation, CMMI 1000404 and CMMI 0856091.

REFERENCES

[1] R. Stibitz. Incremental feed mechanisms. *U.S. Patent*, 1964.
[2] N. Shimizu, T. Kimura, T. Nakamura, and I. Umebu. An ultrahigh vacuum scanning tunneling microscope with a new inchworm mechanism. *Journal of Vacuum Science and Technology A*, 8(1):333–335, 1990.
[3] D. Jeon and R. F. Willis. Inchworm controller for fine approach in a scanning tunneling microscope. *Journal of Vacuum Science and Technology A*, Jul/Aug, A-9 (4):2418–2419, 1991.
[4] J. C. Fasik. An inchworm actuator for the next generation space telescope. Technical report, Burleigh Instruments, Inc., Fishers, NY, oct 1998.
[5] Bi Zhang and Zhenqi Zhu. Developing a linear piezomotor with nanometer resolution and high stiffness. *IEEE/ASME Transactions on Mechatronics*, 2(1), March:22–29, 1997.
[6] L. Howald, H. Rudin, and H. J. Guntherodt. Piezoelectric inertial stepping motor with spherical rotor. *Review of Scientific Instruments*, 63(8):3909–3912, Aug, 1992.
[7] Q. Zou, C. Vander Giessen, J. Garbini, and S. Devasia. Precision tracking of driving waveforms for inertial reaction devices. *Review of Scientific Instruments by the American Institute of Physics*, 76(2):Article No. 023701 (Pages 1–9), February 2005.
[8] Yingchun Zhang, Guangjun Liu, and Juergen Hesselbach. On development of a rotary-linear actuator using piezoelectric translators. *IEEE-ASME Transactions on Mechatronics*, 11(5):647–650, OCT, 2006.
[9] D. K. LINDNER, K. M. REICHARD, and L. M. TARKENTON. Zeros of modal models of flexible structures. *IEEE Trans. on Automatic Control*, 38(9):1384–1388, 1993.
[10] S. Devasia, E. Eleftheriou, and S. O. Reza Moheimani. A survey of control issues in nanopositioning. *IEEE Transactions on Control Systems Technology*, 15(5):802–823, Sept, 2007.
[11] N. Tamer and M. A. Dahleh. Feedback control of piezoelectric tube scanners. *Proceedings of Control and Decision Conference, Lake Buena Vista, Florida*, pages 1826–1831, 1994.
[12] A. Daniele, S. Salapaka, M.V. Salapaka, and M. Dahleh. Piezoelectric scanners for atomic force microscopes: Design of lateral sensors, indentification and control. In *Proceedings of the American Control Conference*, pages 253–257, San Diego, CA, June 1999.
[13] G. Schitter, P. Menold, H. F. Knapp, F. Allgower, and A. Stemmer. High performance feedback for fast scanning atomic force microscopy. *Rev. Sci. Instrum.*, 72(8):3320–3327, 2001.
[14] S. Bashash and N. Jalili. A polynomial-based linear mapping strategy for feedforward compensation of hysteresis in piezoelectric actuators. *Journal of Dynamic Systems Measurement and Control*, 130(3):1–10, Article # 031008, May, 2008.
[15] S. Salapaka, A. Sebastian, J. P. Cleveland, and M. V. Salapaka. High bandwidth nano-positioner: A robust control approach. *Review of Scientific Instruments*, 73(9):3232–3241, Sept., 2002.
[16] G. Schitter, K. J. Aström, B. E. DeMartini, P. J. Thurner, K. L. Turner, and P. K. Hansma. Design and modeling of a high-speed AFM-scanner. *IEEE Transactions on Control Systems Technology*, 15(5):906–915, September, 2007.
[17] Y. Ando, T. Ikehara, and S. Matsumoto. Development of three-dimensional microstages using inclined deep-reactive ion etching. *Journal of Microelectromechanical systems*, 16(3):748–751, June, 2007.
[18] K. K. Leang and A. J. Fleming. High-speed serial-kinematic AFM scanner: Design and drive considerations. *Proceedings of American Control Conference, Seattle, WA*, pages 3188–3193, June 11-13, 2008.
[19] Shih-Hui Chao, J. L. Garbini, and W. M. Dougherty. The design and control of a three-dimensional piezoceramic tube scanner with an inertial slider. *Review of Scientific Instruments*, 77:Article # 063710, 2006.
[20] Y. Yan, Y. Wu, Q. Zou, and C. Su. An integrated approach to piezoactuator positioning in high-speed atomic force microscope imaging. *Review of Scientific Instruments*, 79(7):Article # 073704, 2008.
[21] K. K. Leang Q. Zou G. M. Clayton, S. Tien and S. Devasia. A review of feedforward control approaches in nanopositioning for high speed spm. *ASME Jounrnal of Dynamic Systems, Measurement and Control, Special Issue on Dynamic Modeling, Control and Manipulation at the Nanoscale*, 131(6):1–19, Nov, 2009.
[22] L Meirovitch. *Fundamentals of Vibrations*.
[23] R.C. Hibbler. *Mechanics of Materials*. Pearson, Prentice Hall.
[24] K Uchino. *Piezoelectric Actuators and Ultrasonic Motors*. Kluwer Academic Publishers.